Physica D 402 (2020) 132229

Contents lists available at ScienceDirect

Physica D

journal homepage: www.elsevier.com/locate/physd

Irreversible energy transfer, localization and non-reciprocity in weakly coupled, nonlinear lattices with asymmetry

Chongan Wang *, Sameh Tawfick, Alexander F. Vakakis

Department of Mechanical Science and Engineering, University of Illinois at Urbana - Champaign, United States of America

ARTICLE INFO

Article history:
Received 25 August 2019
Received in revised form 1 October 2019
Accepted 10 October 2019
Available online 18 October 2019
Communicated by C. Josserand

Keywords:
Coupled nonlinear lattices
Passive energy redirection
Landau–Zener tunneling

ABSTRACT

A semi-infinite network of two coupled semi-infinite nonlinear lattices is studied, having the capacity for passive irreversible energy transfer (redirection) from an "excited lattice" (forced by an impulse) to an "absorbing lattice" (that is not directly forced). This is achieved by breaking the symmetry through a spatial variation of the grounding stiffnesses of the excited lattice from the second unit cell onwards, and assuming weak coupling. We show analytically that irreversible energy transfer is caused by the macroscopic analogue (in space) of the Landau–Zener tunneling (LZT) effect, which originated in quantum mechanics in the context of linear parametric oscillators (in time). By constructing a reduced-order model (ROM) of two coupled oscillators it is possible to theoretically model the LZT-induced irreversible energy redirection from the excited to the absorbing lattice. A computational study reveals that the LZT effect is realized only in a critical band of energy, while outside this band there occurs energy localization. The lower and upper energy bounds of this critical band are theoretically approximated by constructing appropriate ROMs of the coupled lattices and studying the bifurcations in their dynamics with energy. This analysis sheds physical insight on the different regimes of the acoustics, and theoretical predictions agree well with direct numerical simulations of the full lattice network. Finally, we show that the LZT effect induces strong non-reciprocity in the dynamics of the finite asymmetric lattice network, in the sense that the impulsive response of this network depends crucially on the forcing-measurement locations and energy. The implications and the possible applications of these results are discussed.

1. Introduction

Certain one-dimensional (1D) nonlinear lattices – e.g., Klein–Gordon and homogeneous granular lattices – support energy-dependent traveling discrete breathers, i.e., oscillatory wavepackets with slowly varying envelopes [1–9]. The "effective particle" approach has been used to study propagating breathers in coupled lattices, by reducing the acoustics to coupled nonlinear oscillators [10]. *Recurrent energy exchanges* through propagating breathers have been studied in coupled Klein–Gordon [11] and granular lattices [9]. Hence, it is natural to ask if it is possible to achieve *irreversible energy transfer* (or equivalently, *energy redirection*) in such coupled lattices. Hasan et al. [12] showed that, indeed this is possible in two coupled, elastically grounded granular lattices under impulse excitation. To achieve this, an asymmetry in the grounding stiffness distribution of the lattice where the impulse was applied (the "excited" lattice) was introduced, and the energy was irreversibly redirected to the other, "absorbing" lattice. The governing nonlinear mechanism was the *spatial macroscopic analogue of the Landau–Zener tunneling effect (LZT)*, first detected in linear quantum mechanical oscillators under parametric excitation [13–15].

We aim to study LZT-induced irreversible energy transfer in a semi-infinite lattice network of two weakly coupled, and linearly grounded 1D lattices with asymmetry and strong nonlinearity under impulse excitation. The individual lattices support propagating breathers [16]. Through analytical and numerical studies, we will prove irreversible energy transfer and energy localization in this network, study their energy dependence and the bifurcations that govern them. Moreover, we will relate these nonlinear phenomena to the break of acoustic reciprocity in the finite asymmetric network and develop measures to quantify it. Finally, we will discuss the implications and possible applications of these findings.

* Corresponding author.
E-mail address: chongan2@illinois.edu (C. Wang).

https://doi.org/10.1016/j.physd.2019.132229
0167-2789/

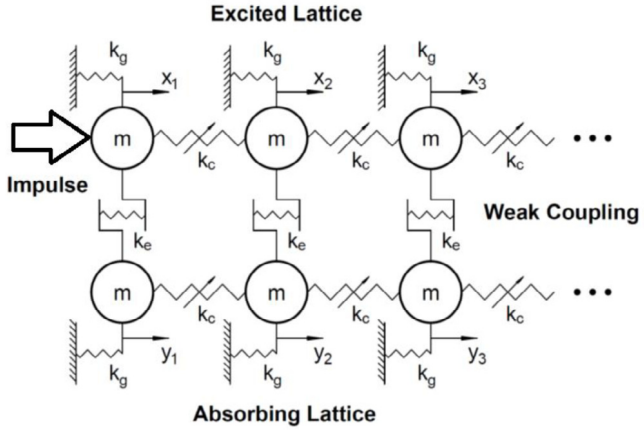

Fig. 1. Schematic of the symmetric lattice network.

Table 1
System parameters for the preliminary series of numerical simulations.

Parameter	m (kg)	k_g (N/m)	k_c (N/m^3)	k_e (N/m)
Value	0.022	1467.27	2.48E9	92.21

2. Irreversible energy transfer and localization in the lattice network

In Fig. 1 we depict the semi-infinite lattice network, composed of two identical 1D lattices of linearly grounded, undamped oscillators coupled to their next neighbors through essentially nonlinear (i.e., non-linearizable) cubic stiffnesses. The two lattices are weakly coupled through linear stiffnesses connecting the corresponding oscillators of each lattice. An impulsive excitation is applied at $t = 0$ – to the leading oscillator of one of the lattices – the "excited lattice" – while the other, "absorbing lattice", is not directly forced. This is equivalent to an initial velocity of the excited oscillator at $t = 0+$ with all other oscillations assumed at rest. We are interested only in *primary wave transmission*, and not be concerned by reflections at the boundaries. As a first step, we assume that *the lattice network is symmetric*, and study its nonlinear acoustics, focusing on energy exchanges between the two lattices. The equations of motion of the symmetric lattice network are then given by,

$$\begin{aligned} m\ddot{x}_1 + k_g x_1 &= -k_c (x_1 - x_2)^3 + k_e (y_1 - x_1) \\ m\ddot{y}_1 + k_g y_1 &= -k_c (y_1 - y_2)^3 + k_e (x_1 - y_1) \\ m\ddot{x}_n + k_g x_n &= k_c \left[(x_{n-1} - x_n)^3 - (x_n - x_{n+1})^3\right] + k_e (y_n - x_n)\,, n \geq 2 \\ m\ddot{y}_n + k_g y_n &= k_c \left[(y_{n-1} - y_n)^3 - (y_n - y_{n+1})^3\right] + k_e (x_n - y_n)\,, n \geq 2 \end{aligned} \tag{1}$$

where x_n and y_n are the displacements of the nth oscillators of the excited and absorbing lattices, respectively, m and k_g their mass and grounding stiffness, k_c the coefficient of the cubic coupling stiffness, and $k_e \ll k_g A^2$ the coefficient of the weak linear coupling stiffness, with A being a characteristic displacement. The initial conditions of (1) are $\dot{x}_1(0+) = v_0$, and zero otherwise. Each lattice is composed of 50 oscillators, and the system parameters are listed in Table 1 with $v_0 = 0.06$ m/s. These parameters correspond to the practical realization of a similar 1D nonlinear lattice [17].

In Fig. 2 we depict the spatio-temporal evolution of the normalized (with respect to the impulsive energy) energies of the two lattices. There are two breathers propagating in the two lattices, with a constant phase difference, revealing the *reversible* mechanism of energy exchange between the lattices in a recurrent and periodic fashion. Each breather is an oscillatory wavepacket with a "fast frequency" that is modulated by a "slow-varying" localized envelope. The recurrent energy exchanges are due to the symmetry and weak coupling of the lattice network of Fig. 1 [9], with the breathers realized under condition of *1:1 resonance*, i.e., all oscillators possess an identical fast frequency. *Then, it is natural to ask under what conditions (perturbations) it is possible to achieve instead irreversible energy transfer in this network*. Hasan et al. [12] answered this question for a granular network by *breaking its symmetry while retaining weak coupling*. A similar approach is adopted here for the lattice network of Fig. 1.

The asymmetric lattice network is depicted in Fig. 3. It is identical to the network of Fig. 1 but for a symmetry-breaking spatial variation of the linear grounding stiffnesses of the oscillators of the excited lattice, i.e., except for the leading oscillator all the other oscillators of that lattice have uniform softer grounding stiffness. This yields the equations of motion,

$$\begin{aligned} m\ddot{x}_1 + k_{g1} x_1 &= -k_c (x_1 - x_2)^3 + k_e (y_1 - x_1) \\ m\ddot{y}_1 + k_{g1} y_1 &= -k_c (y_1 - y_2)^3 + k_e (x_1 - y_1) \\ m\ddot{x}_n + k_{g1} x_n &= k_c \left[(x_{n-1} - x_n)^3 - (x_n - x_{n+1})^3\right] + k_e (y_n - x_n)\,, n \geq 2 \\ m\ddot{y}_n + k_{g2} y_n &= k_c \left[(y_{n-1} - y_n)^3 - (y_n - y_{n+1})^3\right] + k_e (x_n - y_n)\,, n \geq 2 \end{aligned} \tag{2}$$

where k_{g1} and $k_{g2} < k_{g1}$ are the original and spatially varied linear grounding stiffness, with $k_{g1} = 1467.27$ N/m and $k_{g2} = 687.53$ N/m (all other system parameters are listed in Table 1), and $v_0 = 0.06$ m/s, i.e., identical to the previous simulation.

In Fig. 4 we depict the spatio-temporal evolutions of the normalized energies of the two lattices and deduce irreversible energy transfer from the excited to the absorbing lattice, with simultaneous initiation of a propagating breather in the absorbing lattice. Energy

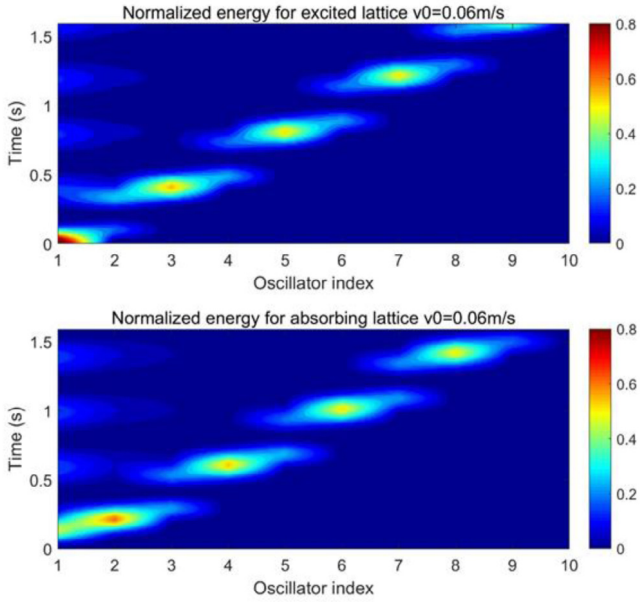

Fig. 2. Spatiotemporal evolution of the normalized energy of the lattices of the symmetric network showing recurrent energy exchanges between lattices ($v_0 = 0.06$ m/s).

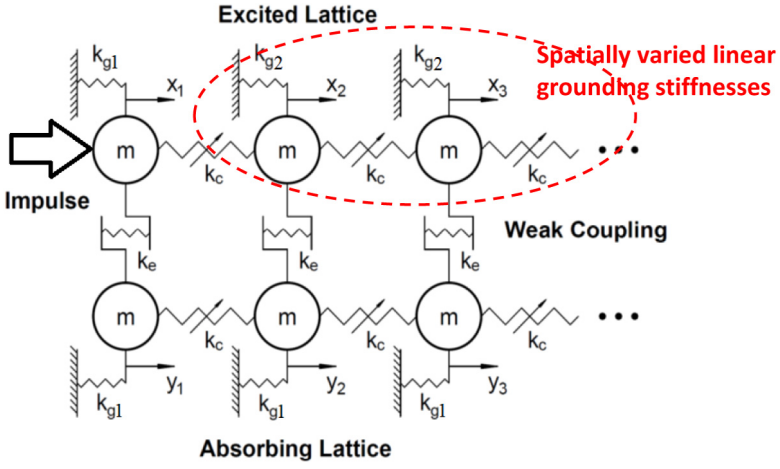

Fig. 3. Schematic of the asymmetric lattice network.

localization is noted in the excited lattice, which rapidly loses its energy following the application of the impulse. The macroscopic spacial analogue of the Landau–Zener Tunneling (LZT) quantum effect which is responsible for irreversible energy transfer will be studied in detail in the next Sections. In addition, *since the asymmetric lattice network of* Fig. 3 *is a strongly nonlinear system, its acoustics depend strongly on the input energy* (i.e., the intensity of the applied impulse). This is shown in Fig. 5 where the "energy penetration" in the asymmetric lattice network is studied for varying impulse intensity. In particular, we depict the contour plots of the maximum instantaneous normalized energy (with respect to input energy) over a certain time period for each of the leading 10 oscillators at a given velocity v_0. The nonlinear acoustics are categorized into four Regimes, labeled as I–IV in Fig. 5, along with some non-robust local effects. The spatio-temporal evolutions of the normalized energies of the two lattices of these different regimes are shown in Appendix A. Regime I corresponds to low-intensity impulses with the energy being localized in the leading oscillators of the excited and absorbing lattices. For intermediate impulses Regime II is realized corresponding to LZT irreversible energy redirection from the excited to the absorbing lattice, and breather propagation in the far field of the absorbing lattice (e.g., Fig. 4 corresponding to $v_0 = 0.06$ m/s). By increasing further the intensity of the impulse Regime III is realized with energy localized in the leading oscillator of the excited lattice. For very high-intensity impulses – Regime IV – there is still no energy transfer from the excited to the absorbing lattice, but there exist propagating breathers in the excited lattice.

These results show that passive energy redirection can be realized only at an intermediate energy band, and below or above that band there occurs energy localization. In Section 3 we construct a reduced-order model (ROM) to prove that irreversible energy transfer in Regime II is due to the LZT effect in space, and in Section 4, we analyze the bifurcations (with respect to energy) that governs the transition from the energy localization to irreversible energy transfer (Regions I to II) and vice versa (Regions II to III). A ROM is constructed for each of the bifurcation.

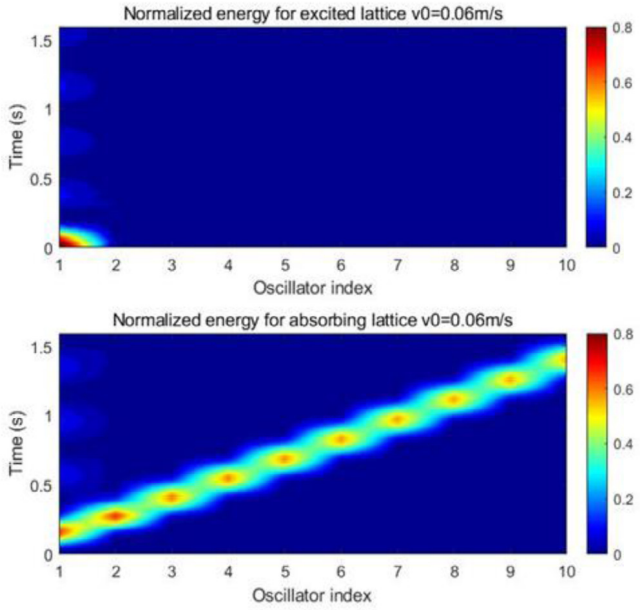

Fig. 4. Spatiotemporal evolution of the normalized energy of the lattices of the asymmetric network showing irreversible energy transfer between lattices ($v_0 = 0.06$ m/s).

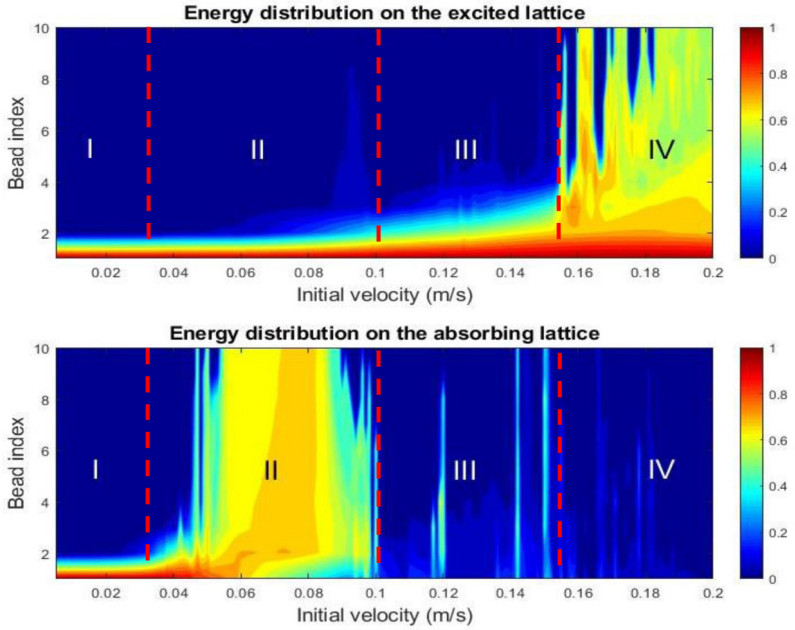

Fig. 5. Normalized energy penetration in the excited and absorbing lattices of the asymmetric network of Fig. 3 for varying impulse intensity; Regimes I–IV of the nonlinear acoustics are indicated, with LZT-induced irreversible energy transfer occurring in Regime II.

3. Irreversible energy transfer in the asymmetric lattice network in Region I

From the asymmetric lattice network of Fig. 3 we denote γ *as the reduction ratio of the grounding stiffnesses*, $0 \leq \gamma \equiv \left(k_{g1} - k_{g2}\right)/k_{g1} < 1$. When $\gamma = 0$ energy is reversibly exchanged between the two lattices in the form of propagating breathers (cf. Fig. 2), whereas when $\gamma > 0$ irreversible energy transfer from the excited to the absorbing lattice is possible. Motivated by the analysis in [12] we require that γ is of the same small order as the weak coupling and the coefficient of the nonlinear stiffnesses, and impose condition of 1:1 resonance; that is all oscillators are assumed to possess the same fast frequency of oscillation. Then, we normalize the equations of motion (2) as follows,

$$\begin{aligned} \ddot{x}_1 + x_1 &= -\varepsilon\alpha\,(x_1 - x_2)^3 + 2\varepsilon\beta y_1 \\ \ddot{y}_1 + y_1 &= -\varepsilon\alpha\,(y_1 - y_2)^3 + 2\varepsilon\beta x_1 \\ \ddot{x}_n + x_n &= \varepsilon\alpha\left[(x_{n-1} - x_n)^3 - (x_n - x_{n+1})^3\right] + 2\varepsilon\beta y_n,\ n \geq 2 \\ \ddot{y}_n + (1 - \varepsilon\gamma)\,y_n &= \varepsilon\alpha\left[(y_{n-1} - y_n)^3 - (y_n - y_{n+1})^3\right] + 2\varepsilon\beta x_n,\ n \geq 2 \end{aligned} \tag{3}$$

where $0 < \epsilon \ll 1$ is a small scaling parameter denoting the smallness of the aforementioned parameters, $\tau = \left[\left(k_{g1} + k_e\right)/m\right]^{1/2} t$ is the new normalized time, $\varepsilon\alpha \equiv k_c/k_{g1}$ is the normalized cubic stiffness coefficient, $\varepsilon\beta \equiv k_e/2\left(k_{g1} + k_e\right)$ is the normalized coupling stiffness coefficient, and all derivatives are with respect to τ. Moreover, assuming that the velocity of the leading oscillator of the excited lattice at $t = 0+$ following the application of the impulse is v_0, the corresponding normalized velocity is $\dot{x}_1\left(\tau = 0+\right) = v_0/\omega$, where $\omega = \left[\left(k_{g1} + k_e\right)/m\right]^{1/2}$, and all other initial conditions are zero. Applying the condition of 1:1 resonance, we follow the complexification-averaging method (CX-A) approach [12,18], and introduce the complex variables (with $i = \sqrt{-1}$),

$$\psi_n^x = \dot{x}_n + ix_n,\ \psi_n^y = \dot{y}_n + iy_n,\ n = 1, 2, \ldots \tag{4}$$

with all oscillators possessing a normalized fast frequency equal to unity. In terms of these new variables the real, second order differential equations (3) are transformed to an equivalent system of complex, first order differential equations,

$$\begin{aligned}
\frac{d\psi_1^x}{dt} - i\psi_1^x &= -\alpha\epsilon\left[\frac{\left(\psi_1^x - \overline{\psi}_1^x\right)}{2i} - \frac{\left(\psi_2^x - \overline{\psi}_2^x\right)}{2i}\right]^3 - i\beta\epsilon\left(\psi_1^y - \overline{\psi}_1^y\right)\\
\frac{d\psi_1^y}{dt} - i\psi_1^y &= -\alpha\epsilon\left[\frac{\left(\psi_1^y - \overline{\psi}_1^y\right)}{2i} - \frac{\left(\psi_2^y - \overline{\psi}_2^y\right)}{2i}\right]^3 - i\beta\epsilon\left(\psi_1^x - \overline{\psi}_1^x\right)\\
\frac{d\psi_n^x}{dt} - i\psi_n^x &= \alpha\epsilon\left\{\left[\frac{\left(\psi_{n-1}^x - \overline{\psi}_{n-1}^x\right)}{2i} - \frac{\left(\psi_n^x - \overline{\psi}_n^x\right)}{2i}\right]^3 - \left[\frac{\left(\psi_n^x - \overline{\psi}_n^x\right)}{2i} - \frac{\left(\psi_{n+1}^x - \overline{\psi}_{n+1}^x\right)}{2i}\right]^3\right\}\\
&\quad -i\beta\epsilon\left(\psi_n^y - \overline{\psi}_n^y\right) - \tfrac{i\gamma}{2}\epsilon\left(\psi_n^x - \overline{\psi}_n^x\right),\ n \geq 2\\
\frac{d\psi_n^y}{dt} - i\psi_n^y &= \alpha\epsilon\left\{\left[\frac{\left(\psi_{n-1}^y - \overline{\psi}_{n-1}^y\right)}{2i} - \frac{\left(\psi_n^y - \overline{\psi}_n^y\right)}{2i}\right]^3 - \left[\frac{\left(\psi_n^y - \overline{\psi}_n^y\right)}{2i} - \frac{\left(\psi_{n+1}^y - \overline{\psi}_{n+1}^y\right)}{2i}\right]^3\right\}\\
&\quad -i\beta\epsilon\left(\psi_n^x - \overline{\psi}_n^x\right),\ n \geq 2
\end{aligned} \tag{5}$$

where overbar denotes the complex conjugate. Anticipating slow and fast time scales in the solution, we asymptotically approximate the irreversible energy transfer employing the method of multiple scales [19], introducing (to leading order) the *fast time scale* $\tau_0 = \tau$ and the *slow time scale* $\tau_1 = \epsilon\tau$, and expressing the solutions in the series forms:

$$\psi_n^x = \psi_{n0}^x + \epsilon\psi_{n1}^x + O\left(\varepsilon^2\right),\quad \psi_n^y = \psi_{n0}^y + \epsilon\psi_{n1}^y + O\left(\varepsilon^2\right),\quad n = 1, 2, \ldots \tag{6}$$

Substituting (5) into (4), expressing the time derivatives in terms of the new time scales, and separating terms of different orders of the small parameter we obtain a hierarchy of linear subproblems. The $O(1)$subproblem reads (for $n = 1, 2, \ldots$),

$$\begin{aligned}
\frac{\partial\psi_{n0}^x}{\partial\tau_0} - i\psi_{n0}^x = 0 &\Rightarrow \psi_{n0}^x = \varphi_{n0}^x\left(\tau_1\right)e^{i\tau_0}\\
\frac{\partial\psi_{n0}^y}{\partial\tau_0} - i\psi_{n0}^y = 0 &\Rightarrow \psi_{n0}^y = \varphi_{n0}^y\left(\tau_1\right)e^{i\tau_0}
\end{aligned} \tag{7}$$

indicating that, to leading order, the responses of the asymmetric lattice network can be expressed in terms of fast oscillations that are modulated by the slow-varying complex envelopes $\varphi_{n0}^{x,y}\left(\tau_1\right)$. These are approximated by eliminating the secular terms from the $O(\epsilon)$ subproblems [19], yielding the following modulation equations or *slow flow*,

$$\begin{aligned}
\frac{\partial\varphi_{10}^x}{\partial\tau_1} &= \frac{3}{8}\alpha i\left|\delta_1^x\right|^2\delta_1^x - i\beta\varphi_{10}^y\\
\frac{\partial\varphi_{10}^y}{\partial\tau_1} &= \frac{3}{8}\alpha i\left|\delta_1^y\right|^2\delta_1^y - i\beta\varphi_{10}^x\\
\frac{\partial\varphi_{n0}^x}{\partial\tau_1} &= \frac{3}{8}\alpha\left\{(-i)\left|\delta_{n-1}^x\right|^2\delta_{n-1}^x - (-i)\left|\delta_n^x\right|^2\delta_n^x\right\} - i\beta\varphi_{n0}^y - \frac{i\gamma}{2}\varphi_{n0}^x,\ n \geq 2\\
\frac{\partial\varphi_{n0}^y}{\partial\tau_1} &= \frac{3}{8}\alpha\left\{(-i)\left|\delta_{n-1}^y\right|^2\delta_{n-1}^y - (-i)\left|\delta_n^y\right|^2\delta_n^y\right\} - i\beta\varphi_{n0}^x,\ n \geq 2
\end{aligned} \tag{8}$$

where $\delta_n^{x,y} \equiv \varphi_{n0}^{x,y} - \varphi_{(n+1)0}^{x,y}$ are the differences between the complex envelopes of neighboring oscillators in the two lattices.

As confirmed by the plots of Fig. 6 (corresponding to the asymmetric lattice network discussed in Section 2), the slow flow (8) predicts irreversible energy transfer from the excited to the absorbing lattice. We note that rapid and complete energy transfer – it occurs within approximately half of a cycle of the oscillation – is initiated immediately after the impulse in applied, through 1:1 resonance interaction between the leading oscillators of the two lattices. This is followed by breather formation and propagation in the absorbing lattice through which energy is transferred to the far field.

We now develop a reduced-order model (ROM) to better understand the nonlinear mechanism governing irreversible energy transfer in the asymmetric lattice network under condition of 1:1 resonance. To this end, we surmise that 1:1 resonance causes the initial intense energy transfer from the leading oscillator of the excited lattice to the leading oscillator of the absorbing lattice, but once this initial energy transfer is completed, the 1:1 resonance is "broken" so that the energy cannot transfer back to the excited lattice. This effect is exactly the spatial analogue of the temporal Landau–Zener Tunneling effect (LZT), where a quantum system under condition of

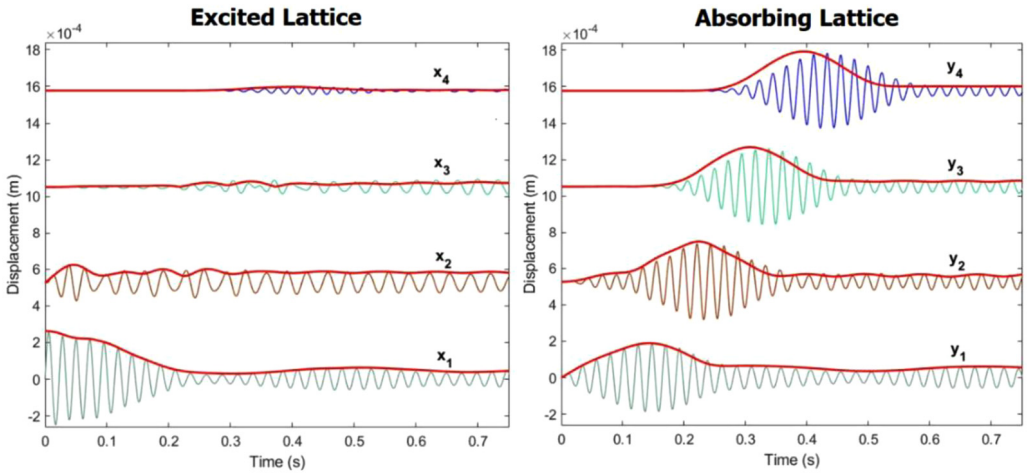

Fig. 6. Regime II of irreversible energy transfer for $v_0 = 0.07$ m/s: Comparison between the exact time series of the four leading oscillators of each lattice obtained by numerical integration of system (3), and the envelopes predicted by the slow flow (8) (red solid lines).

resonance tunnels energy across an energy gap between two anti-crossed energy levels for a finite period of time, before the resonance condition breaks trapping the transferred energy [13,14]. Manevitch et al. [15] demonstrated this quantum mechanical effect in the macroscale by means of two coupled pendulums with the length of one of the pendulums varying linearly in time, showing theoretically and experimentally irreversible energy trapping.

Accordingly, *we will develop an "effective particle" ROM to reduce the nonlinear acoustics of the spatially asymmetric lattice network to a linear time-varying system of two coupled oscillators from which the LZT effect could be immediately discerned* [12,15]. To this end, we assume that energy propagates along the two lattices in the form of breathers with constant speed under condition of 1:1 resonance, so that *the energy is localized at one oscillator at a given time*. Therefore the excited and absorbing lattices can be replaced by two oscillators: As the absorbing lattice has spatially uniform grounding stiffness, the grounding stiffness of the "absorbing oscillator" is constant (time-invariant); however, since the grounding stiffness of the excited lattice varies as the breather propagates, the "excited oscillator" possesses time-varying grounding stiffness. To construct the ROM we introduce the new variables,

$$u = \sum_{n=1}^{+\infty} x_n, \quad v = \sum_{n=1}^{+\infty} y_n \tag{9}$$

and add the two sets of Eq. (3) to obtain the following *linear* differential equations,

$$\begin{aligned} \ddot{u} + (1-\varepsilon\gamma)\,u + \varepsilon\gamma x_1 &= 2\beta\varepsilon v \\ \ddot{v} + v &= 2\beta\varepsilon u \end{aligned} \tag{10}$$

where the nonlinear terms have canceled by the summation. Eq. (10) are exact up to this point, but to derive the ROM in its final form it is necessary to express $x_1(\tau)$ in terms of the variables (9). This can only be accomplished approximately, e.g., by introducing the functional relationship $x_1(\tau) = \xi(\tau)\,u(\tau)$. Then, assuming that the impulsive energy is irreversibly transferred completely from the excited to the absorbing oscillator, the function $\xi(\tau)$ can be approximated following a three-stage approach. First, the energy is assumed to be localized entirely in the leading oscillators of the excited and absorbing lattices so that all other oscillators have zero response and $u(\tau) \approx x_1(\tau) \Rightarrow \xi(\tau) \approx 1$. Following that, there is initiation of the propagating breather in the absorbing lattice, i.e., of nearly complete energy transfer from the leading oscillator of that lattice to its neighboring oscillator, so $\xi(\tau)$ can be assumed to linearly decrease in the range $1 \geq \xi(\tau) \geq 0$. Finally, after the propagating breather has been initiated, energy propagates in the absorbing lattice, and $\xi(\tau) \approx 0$. Hence, we arrive to the final form of the ROM, in the form of the linear, time-varying system,

$$\begin{aligned} \ddot{u}(\tau) + (1-\varepsilon\gamma)\,u(\tau) + \varepsilon\gamma\xi(\tau)\,u(\tau) &= 2\beta\varepsilon v(\tau) \\ \ddot{v}(\tau) + v(\tau) &= 2\beta\varepsilon u(\tau) \end{aligned} \tag{11a}$$

where $\xi(\tau)$ is the $O(1)$ piecewise-linear function:

$$\xi(\tau) = \begin{cases} 1 & (\tau \leq c_1) \\ \dfrac{c_1 + c_2 - \tau}{c_2} & (c_1 < \tau \leq c_1 + c_2) \\ 0 & (\tau > c_1 + c_2) \end{cases} \tag{11b}$$

In (11a) the u-oscillator is the excited oscillator, and the v-oscillator the absorbing one. In (11b) c_1 is the time required for the energy to completely transfer from the leading oscillator of the excited lattice to the leading oscillator of the absorbing one, whereas c_2 the time required for the energy to be completely transferred from the leading oscillator of the absorbing lattice to its neighboring oscillator in the same lattice. The initial conditions of the ROM are zero but for the velocity of the excited oscillator, $\dot{u}(0+) = \dot{x}_1(0+) = v_0/\omega$.

The analytical study of the ROM is carried out similarly to the original network (3) by the CX-A method. To this end we introduce the complex variables, $\psi_u = \dot{u} + iu$ and $\psi_v = \dot{v} + iv$, under condition of 1:1 resonance between the two oscillators of the ROM – as in the analysis of (3). As before we introduce the fast and slow time scales, τ_0 and τ_1, respectively, and expand the complex variables as,

$\psi_u = \psi_{u0} + \varepsilon\psi_{u1} + O\left(\varepsilon^2\right)$, and $\psi_v = \psi_{v0} + \varepsilon\psi_{v1} + O\left(\varepsilon^2\right)$. Then, the leading order approximation of the solution is expressed as,

$$\psi_u = \varphi_{u0}\left(\tau_1\right) e^{i\tau_0} + O\left(\varepsilon\right) \psi_v = \varphi_{v0}\left(\tau_1\right) e^{i\tau_0} + O\left(\varepsilon\right) \tag{12a}$$

where the slowly varying complex envelopes are governed by the following *reduced slow flow*,

$$\begin{aligned} 2i\frac{\partial\varphi_{u0}}{\partial\tau_1} &= 2\beta\varphi_{v0} + \gamma\eta\left(\tau_1\right)\varphi_{u0} \\ i\frac{\partial\varphi_{v0}}{\partial\tau_1} &= \beta\varphi_{u0} \end{aligned} \tag{12b}$$

and the parametric, slowly varying term is expressed as:

$$\eta\left(\tau_1\right) \equiv 1 - \xi(\tau_1 - \varepsilon c_1) = \begin{cases} \dfrac{\tau_1}{\varepsilon c_2}, & \varepsilon c_1 \le \tau_1 \le \varepsilon c_2 \\ 1, & \tau_1 > \varepsilon c_2 \end{cases} \tag{12c}$$

We note that the ROM (12a)–(12c) models the acoustics *after* the energy has been transferred from the leading oscillator of the excited lattice to the leading oscillator of the absorbing lattice in the time interval $\tau_1 \le \varepsilon c_1$. Indeed, in writing (12c) we take into account that $\eta\left(\tau_1\right) = 0$ for $\tau_1 \le \varepsilon c_1$, during which time there occurs complete energy transfer from the excited to the absorbing oscillator through a linear beat phenomenon under condition of 1:1 resonance. At $\tau_1 = \varepsilon c_1$ energy transfer has been completed to the leading oscillator of the absorbing lattice, so the initial conditions for (12b) are $\varphi_{u0}\left(0\right) = 0$ and $\varphi_{v0}\left(0\right) = 1$. For $\varepsilon c_1 \le \tau_1 \le \varepsilon c_2$ energy gets transferred from the leading oscillator to the other oscillators of the absorbing lattice, whereas for $\tau_1 > \varepsilon c_2$ the breather in the absorbing lattice has been initiated. In addition note from (12b) that, if $\gamma \gg \beta$, for $\tau_1 > \varepsilon c_1$ the condition for 1-1 resonance is gradually broken, and the energy remains mainly localized in the absorbing lattice – some small amount is expected to "leak back" to the excited oscillator through the small coupling term in the first of Eq. (12b) – since there is no resonance mechanism to transfer it back to the exciting lattice. Hence, *the acoustics of the asymmetric lattice network reduced to the ROM (12a)–(12c) is proven to be governed by the LZT effect*; moreover, the spatial stiffness asymmetry shown in Fig. 3 – which in the ROM (12a)–(12b) is transformed to time-varying stiffness asymmetry – serves as the mechanism that breaks 1:1 resonance and ensures the irreversibility of the energy transfer.

The ROM (12a)–(12b) can be explicitly solved by defining the ratio $a = \gamma/\varepsilon c_2$, and combining the complex equations (12b) into a linear complex equation in terms of the response of the absorbing oscillator,

$$\frac{d^2\varphi_{v0}}{d\tau_1^2} + \frac{i\tau_1 a}{2}\frac{d\varphi_{v0}}{d\tau_1} + \beta^2\varphi_{v0} = 0 \tag{13}$$

with initial conditions $\varphi_{v0}\left(0\right) = 1$ and $\frac{d\varphi_{v0}(0)}{d\tau_1} = 0$. Through the transformations, $\Phi = \varphi_{v0}(\tau_1) exp\left(ia\tau_1^2/8\right)$, $z = \tau_1\left(a/2\right)^{1/2} exp\left(-i\pi/4\right)$, $\nu = 2i\beta^2/a$, the system (13) is expressed as,

$$\frac{d^2\Phi}{dz^2} + \left(\nu + \frac{1}{2} - \frac{z^2}{4}\right)\Phi = 0 \tag{14}$$

with initial conditions $\Phi\left(0\right) = 1$, $\Phi'\left(0\right) = 0$. Eq. (14) is the normal form of Weber's equation [20] which admits an explicit asymptotic solution in terms of tabulated functions. As it is a linear, homogeneous, second-order differential equation, its general solution is expressed as a linear combination of two fundamental solutions,

$$\Phi(z) = C_1 D_{-\nu-1}\left(iz\right) + C_2 D_{-\nu-1}\left(-iz\right) \tag{15a}$$

where $D_{-\nu-1}\left(\pm iz\right)$ are Weber's functions with well-defined asymptotic behaviors [20] as $z \to +\infty$ (or $\tau_1 \to +\infty$):

$$\begin{aligned} \lim_{z\to+\infty} D_{-\nu-1}\left(iz\right) &= 0 \\ D_{-\nu-1}\left(-iz\right) &\sim \frac{\sqrt{2\pi}}{\mathrm{G}\left(\nu+1\right)} e^{\pi\nu i/4} e^{i|z|^2/4} |z|^{\nu}, \qquad z \to +\infty \end{aligned} \tag{15b}$$

Imposing the previous initial conditions, we may evaluate the two unknown constants C_1 and C_2 as follows:

$$\begin{aligned} C_1 &= \frac{2^{\nu/2}\sqrt{2\pi}}{\pi\Gamma\left(-\nu/2\right)} \cos\frac{\pi\left(\nu+1\right)}{2} - \Gamma\left(-\nu\right)\ \Gamma\left(\nu+1\right) \sin\frac{\pi\left(\nu+1\right)}{2} \sin\pi\left(\nu+\frac{1}{2}\right) \\ C_2 &= \frac{2^{\nu/2}\sqrt{2\pi}}{\pi\Gamma\left(-\nu/2\right)}\ \Gamma\left(-\nu\right)\ \Gamma\left(\nu+1\right) \sin\frac{\pi\left(\nu+1\right)}{2} \end{aligned} \tag{15c}$$

Relations (15a)–(15c) provide an exact analytic expression for the leading-order response of the absorbing oscillator, $\varphi_{v0}(\tau_1)$, and through the first of relations (12b), also of the corresponding response of the excited oscillator, $\varphi_{u0}(\tau_1)$. To study the energy transfer in the asymmetric lattice network (caused by the spatial variation of the grounding stiffness distribution of the excited lattice), it is of interest to consider the leading-order approximations of the energies of the two oscillators of the ROM as $\tau_1 \to +\infty$. These are analytically evaluated by the squares of φ_{v0} and φ_{u0}, yielding the following asymptotic expression of the energy that is irreversibly transferred to the absorbing oscillator,

$$\lim_{\tau_1\to+\infty} |\varphi_{v0}\left(\tau_1\right)|^2 = \lim_{z\to+\infty} |\Phi\left(z\right)|^2 = \frac{1 + e^{-\frac{2\pi\beta^2}{a}}}{2} = \frac{1 + e^{-\frac{2\pi\beta^2\varepsilon c_2}{\gamma}}}{2} \tag{16a}$$

where εc_2 is the (unnormalized) time required for the generation of the propagating breather in the absorbing lattice, i.e., the time required for energy to be completely transferred from the leading oscillator of the absorbing lattice to its neighboring oscillator in the

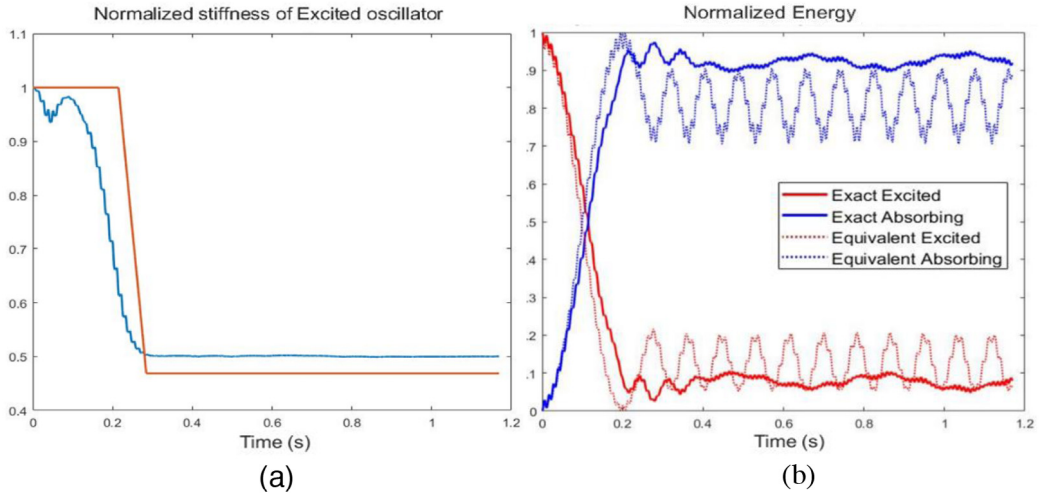

Fig. 7. The ROM (11a), (11b) compared to the asymmetric lattice network (3) for $v_0 = 0.07$ m/s: (a) Weighted-averaged grounded stiffness (17) – blue line, versus the approximation (11b) – red line; (b) instantaneous energies of the excited and absorbing lattices – solid lines, versus the analytical ROM predictions for the excited and absorbing oscillators – dashed lines. (For interpretation of the references to color in this figure legend, the reader is referred to the web version of this article.)

same lattice. This time interval can be approximated by the peak-to-peak time delay of the traveling breather, which was analytically approximated by Mojahed et al. [16] for an infinite lattice with the cubic nonlinearity considered herein as, $\varepsilon\alpha T A^2 = 0.7975/\left(\frac{3}{8}\right) \approx 2.13$, where A is the amplitude of the breather, T the peak-to-peak time delay, and α the normalized coefficient of the cubic nonlinearity. Substituting into (16) we obtain the final expression:

$$\lim_{\tau_1 \to +\infty} |\varphi_{v0}(\tau_1)|^2 = \frac{1 + e^{-\frac{2\pi\beta^2 \times 2.13}{\gamma\alpha A^2}}}{2} \tag{16b}$$

In (16b), the normalized coefficient denoting the strength of the cubic nonlinearity, αA^2, and the normalized coupling stiffness coefficient, β, must be of the same order, or the energy will localize in the leading oscillators of the two lattices (cf. the discussion in the next section). If, in addition, the stiffness reduction ratio γ is sufficiently larger than the normalized coupling coefficient β, i.e. $\gamma \gg \beta$, then $\lim_{\tau_1 \to +\infty} |\varphi_{v0}(\tau_1)|^2 \approx 1$, and nearly all of the impulsive energy becomes irreversibly localized to the absorbing oscillator; otherwise, if $\gamma \ll \beta$, then $\lim_{\tau_1 \to +\infty} |\varphi_{v0}(\tau_1)|^2 \approx 1/2$ and the energy is reversibly and recursively exchanged between the two oscillators in a nonlinear beat phenomenon. This analytical result provides physical insight into the LZT mechanism that governs irreversible energy transfer in the spatially asymmetric lattice network, and fully correlates with the numerical results of the previous section.

As a final step we wish to validate the approximate ROM (11a), (11b) based on numerical simulations of the exact asymmetric lattice network (3). Recall that in the exact network the grounding stiffness of the excited lattice is *spatially varying*, whereas in the ROM the grounding stiffness of the excited oscillator is *time varying*. Therefore, we compute the weighted-averaged grounding stiffness over time, $\bar{k}_g(t)$, of the excited lattice in (3),

$$\bar{k}_g(t) = \frac{\sum_{i=1}^{n} k_{gi} E_i(t)}{E} \tag{17}$$

and compare the result with the analytical approximation (11b). In (17) E is the total energy provided by the impulse, $E_i(t)$ the instantaneous energy of the ith oscillator pair of the excited and absorbing lattices (note that $\sum_{i=1}^{n} E_i(t) = E, t \geq 0$), and k_{gi} the grounding stiffness of the ith oscillator of the excited lattice. From Fig. 7a we note that the difference between the approximate and numerical results is small, validating the ROM. These computations correspond to the asymmetric lattice network of Section 2 with $v_0 = 0.07$ m/s.

Finally, in Fig. 7b we validate the analytical prediction of the ROM regarding irreversible energy transfer by comparing to the results of direct numerical simulations. We note good agreement, especially in the critical, early regime of the response during which irreversible energy transfer from the leading oscillator of the excited lattice to the corresponding oscillator of the absorbing lattice. The small oscillations in the energy values at later times are due to the simplifying assumptions of the ROM, and its inability to more accurately capture the time-varying stiffness of the excited oscillator (note also the small difference between the predicted and exact steady values of the "effective stiffness" of the excited oscillator in Fig. 7a.

As shown in Fig. 5, the intensity of the applied impulse plays a major role in the nonlinear acoustics, causing transitions (bifurcations) between irreversible energy transfer and localization. In the next Section we theoretically study these important effects and provide analytical estimates for the bifurcation energy values that bound the regime of LZT irreversible energy transfer (Regime II in Fig. 5). In the process we aim to shed physical insight into the qualitative changes that occur in the nonlinear acoustics when these bifurcations occur.

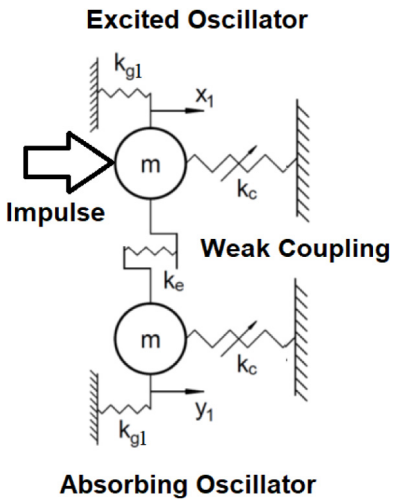

Fig. 8. Two-DOF ROM for the high-energy bifurcation from LZT-induced irreversible energy transfer (Regime II) to localization (Regime III) in the asymmetric lattice network.

4. Bifurcations bounding the Regime II of irreversible energy transfer

First, we consider the high-energy bifurcation from Regime II of LZT-induced irreversible energy transfer to Regime III in Fig. 5. Given that in Regime III most of the energy is localized in the leading oscillator of the excited lattice, *the break of 1:1 resonance (which prevents LZT irreversible energy transfer) is related to the inability of the energy to being transferred from the leading pair of oscillators to the far fields of both lattices;* clearly, this is caused by the asymmetry of the grounding stiffness of the excited lattice after the leading oscillator. Hence, in Regime III the asymmetric lattice network can be approximately replaced by a two-DOF ROM composed of just the two leading oscillators of the excited and absorbing lattices as depicted in Fig. 8, assuming that all remaining oscillators are nearly motionless.

The normalized equations of motion of the two-DOF ROM of Fig. 8 are given by,

$$\begin{aligned} &\ddot{x}_1 + x_1 + \varepsilon\alpha x_1^3 - 2\varepsilon\beta y_1 = 0 \\ &\ddot{y}_1 + y_1 + \varepsilon\alpha y_1^3 - 2\varepsilon\beta x_1 = 0 \end{aligned} \tag{18}$$

Where the notation of the previous section holds, and the initial conditions are zero but for $\dot{x}_1(0+) = v_0/\omega$ Transforming in terms of the linear modal variables $u = (x_1 + y_1)/2$, $v = (x_1 - y_1)/2$, the system (18) is expressed as:

$$\begin{aligned} &\ddot{u} + (1 - \varepsilon 2\beta)\, u + \varepsilon\alpha\left(u^3 + 3uv^2\right) = 0 \\ &\ddot{v} + (1 + \varepsilon 2\beta)\, v + \varepsilon\alpha\left(v^3 + 3u^2 v\right) = 0 \end{aligned} \tag{19}$$

Assuming 1:1 resonance we apply the CX-A method introducing the complex variables $\psi_u^h = \dot{u} + iu$ and $\psi_v^h = \dot{v} + iv$, yielding the following leading order approximations,

$$\psi_u^h = \varphi_u^h(\tau_1)\, e^{i\tau_0} + O(\varepsilon)\, \psi_v^h = \varphi_v^h(\tau_1)\, e^{i\tau_0} + O(\varepsilon) \tag{20a}$$

where the slowly varying complex envelopes are governed by the *high-energy slow flow*,

$$\begin{aligned} &\frac{\partial\varphi_u^h}{\partial\tau_1} + i\beta\varphi_u^h - \frac{3i\alpha}{8}\left[\varphi_u^{h2}\overline{\varphi}_u^h + 2\varphi_u^h\varphi_v^h\overline{\varphi}_v^h + \varphi_v^{h2}\overline{\varphi}_u^h\right] = 0 \\ &\frac{\partial\varphi_v^h}{\partial\tau_1} + i\beta\varphi_v^h - \frac{3i\alpha}{8}\left[\varphi_v^{h2}\overline{\varphi}_v^h + 2\varphi_v^h\varphi_u^h\overline{\varphi}_u^h + \varphi_u^{h2}\overline{\varphi}_v^h\right] = 0 \end{aligned} \tag{20b}$$

with overbar denoting complex conjugate. Expressing the slow complex amplitudes in terms of real amplitudes and phases, $\varphi_u^h = A_u^h e^{i\theta_u^h}$ and $\varphi_v^h = A_v^h e^{i\theta_v^h}$, and realizing that conservation of energy holds, $A_u^{h2} + A_v^{h2} = \rho^2$, we introduce the variable transformations $A_u^h = \rho\cos\psi$ and $A_v^h = \rho\sin\psi$ and reduce (20b) to the following slow flow on a sphere,

$$\begin{aligned} \frac{d\rho}{d\tau_1^*} &= 0 \Rightarrow \rho = const \\ \frac{d\psi}{d\tau_1^*} &= \sin 2\psi \sin 2\phi \\ \frac{d\phi}{d\tau_1^*} &= \delta + 2\cos 2\psi\,[1 + \cos 2\phi] \end{aligned} \tag{20c}$$

where $\tau_1^* = \frac{3\alpha\rho^2}{16}\tau_1$ is a rescaled slow time, $\phi = \theta_v^h - \theta_u^h$, and $(\psi, \phi) \in [0, \pi) \times [0, \pi)$. Note that it suffices to consider the solution only in the domain $(\psi, \phi) \in \left[0, \frac{\pi}{2}\right] \times \left[0, \frac{\pi}{2}\right]$.

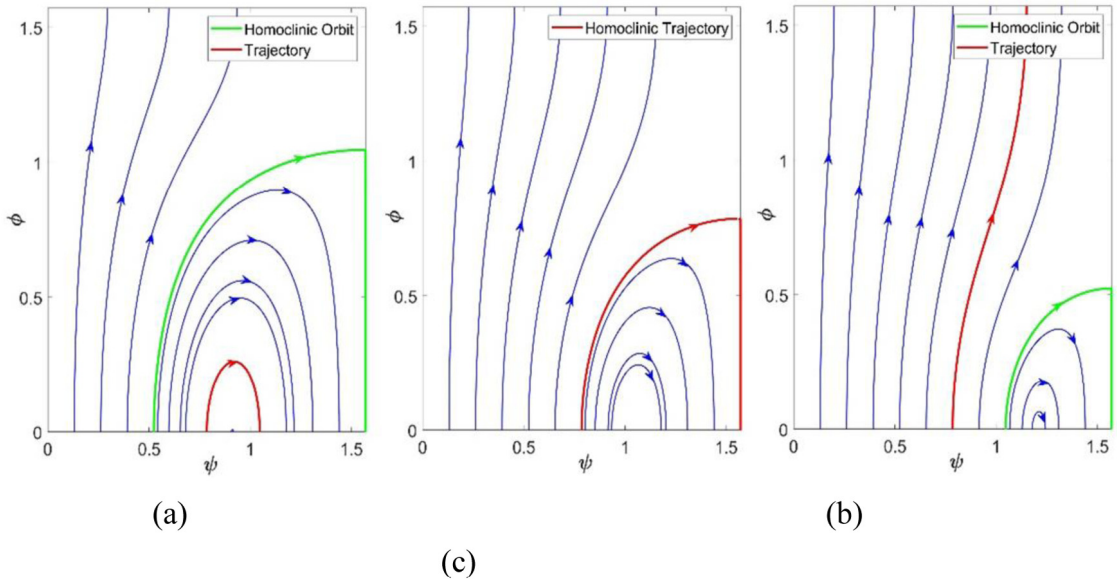

Fig. 9. Bifurcation in the phase plot of the high-energy slow flow (20c): (a) $\delta = 1$, (b) $\delta = 2$, (c) $\delta = 3$; the homoclinic (green line) and "impulsive" orbit (red line) are highlighted. (For interpretation of the references to color in this figure legend, the reader is referred to the web version of this article.)

The initial conditions for (20c) corresponding to impulsive excitation of the excited oscillator are $\psi(0) = \pi/4$ and $\phi(0) = 0$, while $\rho = v_0/\left(2^{1/2}\omega\right)$ relates to the intensity of the impulse. Hence, the slow dynamics of (19) is governed by the bifurcation parameter $\delta = 32\beta/3\alpha\rho^2$. Interestingly, the reduced flow (20c) can be solved analytically since it admits a second constant of motion, $-\sin^2 2\psi \cos 2\phi + \delta \cos 2\psi + \frac{1}{2}\cos 4\psi = H$, and it can be shown that $\delta = 2$ *corresponds to a bifurcation for the slow flow* (20c) as explained below.

For $\delta < 4$ the slow flow has two fixed points, $(\psi_1, \phi_1) = \left(\frac{\pi}{2}, \frac{1}{2}\arccos\left(\frac{1}{2}\delta - 1\right)\right)$ which is an unstable saddle, and $(\psi_2, \phi_2) = \left(\frac{1}{2}\arccos\left(-\frac{\delta}{4}\right), 0\right)$ which is a neutrally stable center. A critical feature is the *homoclinic orbit* connecting the saddle point (ψ_1, ϕ_1) with itself, which is computed by $-\sin^2 2\psi \cos 2\phi + \delta \cos 2\psi + (1/2)\cos 4\psi = -3/2$. In Fig. 9 we depict the slow flow (20c) for three different values of the bifurcation parameter δ, and give emphasis on the relative positioning of the homoclinic orbit and the "impulsive" orbit generated by the specific impulsive excitation of the problem. At the bifurcation value $\delta = 2$ these two orbits coincide, whereas for $\delta < 2$ ($\delta > 2$) the impulsive orbit is located inside (outside) the homoclinic orbit. The repercussions of this topological change on the dynamics of the ROM (18) – and on the acoustics of the asymmetric lattice network (3) – are now discussed.

Note that $u = (x_1 + y_1)/2$ is the response of the in-phase mode, while $v = (x_1 - y_1)/2$ of the out-of-phase mode of the ROM (18). Considering the impulsive orbit, initially $\phi = \theta_v - \theta_u = 0$ with the energy being localized to the excited oscillator x_1. If, as in Fig. 9c, $\phi \to \pi$ with increasing time, the energy gets irreversibly transferred (since there is no recurrence – or oscillation – in ϕ) to the absorbing oscillator y_1; otherwise, if as in Fig. 9a, ϕ undergoes small oscillations the energy remains mainly localized in the excited oscillator and no irreversible energy transfer can occur. The latter (former) occurs as long as the impulsive orbit is located inside (outside) the homoclinic loop. It follows that *the bifurcation in the slow flow at* $\delta = 2$ *corresponds to the change from localization* ($\delta < 2$) *to irreversible energy transfer* ($\delta > 2$). Considering the system parameters of the system of Fig. 3, this bifurcation is predicted at the critical initial velocity $v_{0,cr}^{HE} = 0.119$ m/s in the high-energy regime, compared to the corresponding numerical value of ~ 0.09 m/s from Fig. 5. This discrepancy is attributed to the simplicity of the ROM of Fig. 8, which assumes that in the regime of localization all oscillators in the two lattices beyond the leading ones are motionless. In actuality, though, although the condition of 1–1 resonance is broken there is still some near-field "energy leakage" in the oscillations beyond the leading ones. Accordingly, to refine our result we need to relax the previous assumption by considering ROMs that include additional oscillators; in that case, however, the CX-A will become more complicated and resort to numerical analysis would be more preferable. Numerically we have determined that by considering a four-DOF ROM composed of the two leading oscillators of the excited and absorbing lattices of the asymmetric lattice network of Fig. 3 we can improve the predicted critical bifurcation velocity to $v_{0,cr}^{HE} \approx 0.098$ m/s. The results are shown in Appendix B in detail. This concludes the discussion of the high-energy bifurcation between Regimes II and III, and our focus shifts to the low-energy bifurcation between Regimes I and II of Fig. 5.

This bifurcation changes localization in Regime I to irreversible energy transfer in Regime II as the intensity of the impulse increases (cf. Fig. 5). We deduce a different type of localization in this case compared to the high-energy Regime III. Indeed, in Regime I energy is continuously exchanged between the two leading oscillators of the two lattices, whereas, after the bifurcation (in Regime II) a breather initiates in the absorbing lattice. Hence, the appropriate ROM in this case is composed of the leading oscillator of the excited lattice (denoted by E1) and the two leading oscillators of the absorbing lattice (denoted by A1 and A2). In Regime I a nonlinear beat phenomenon occurs between oscillators E1 and A1, with oscillator A2 being motionless (cf. Fig. 10). In Regime II, however, there is energy transfer from oscillator A1 to A2, as the breather is initiated.

In the low-energy regime we rescale, $x_1 \to \sqrt{\varepsilon}x_1, y_1 \to \sqrt{\varepsilon}y_1, y_2 \to \sqrt{\varepsilon}y_2$ and $v_0 \to \sqrt{\varepsilon}v_0$ to denote the smallness of the displacements and initial velocity of the ROM, yielding the normalized equations of motion,

$$\begin{aligned} \ddot{x}_1 + x_1 + \varepsilon^2\alpha x_1^3 &= 2\varepsilon\beta y_1 \\ \ddot{y}_1 + y_1 + \varepsilon^2\alpha\left(y_1 - y_2\right)^3 &= 2\varepsilon\beta x_1 \\ \ddot{y}_2 + y_2 + \varepsilon^2\alpha\left(y_2 - y_1\right)^3 + \varepsilon^2\alpha y_2^3 &= 0 \end{aligned} \tag{21}$$

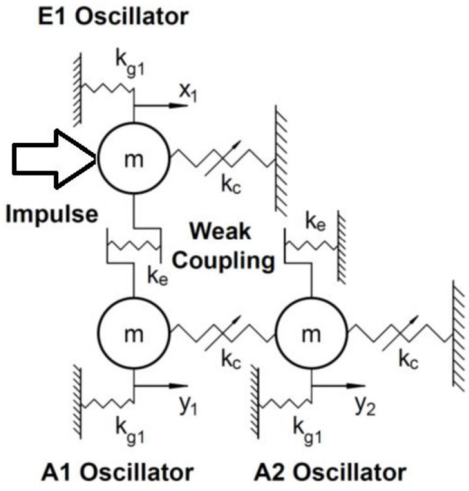

Fig. 10. The ROM for the low-energy bifurcation from localization (Regime I) to LZT-induced irreversible energy transfer (Regime II); the leading oscillator of the excited lattice is denoted by E1, and the two leading oscillators of the absorbing lattice by A1 and A2.

with zero initial conditions but for $\dot{x}_1(0+) = v_0/\omega$. Assuming a regime of 1:1:1 resonance in the responses of the three oscillators the CX-A method is applied again through the complex variables $\psi_1^x = \dot{x}_1 + ix_1$, $\psi_1^y = \dot{y}_1 + iy_1$ and $\psi_2^y = \dot{y}_2 + iy_2$, expressed in series,

$$\begin{aligned}
\psi_1^x &= \psi_{10}^x(\tau_0,\tau_1,\tau_2) + \varepsilon\psi_{11}^x(\tau_0,\tau_1,\tau_2) + \varepsilon^2\psi_{12}^x(\tau_0,\tau_1,\tau_2) + \mathrm{O}\left(\varepsilon^3\right)\\
\psi_1^y &= \psi_{10}^y(\tau_0,\tau_1,\tau_2) + \varepsilon\psi_{11}^y(\tau_0,\tau_1,\tau_2) + \varepsilon^2\psi_{12}^y(\tau_0,\tau_1,\tau_2) + \mathrm{O}\left(\varepsilon^3\right)\\
\psi_2^y &= \psi_{20}^y(\tau_0,\tau_1,\tau_2) + \varepsilon\psi_{21}^y(\tau_0,\tau_1,\tau_2) + \varepsilon^2\psi_{22}^y(\tau_0,\tau_1,\tau_2) + \mathrm{O}\left(\varepsilon^3\right)
\end{aligned} \tag{22}$$

where $\tau_0 = t$, $\tau_1 = \epsilon t$ and $\tau_2 = \epsilon^2 t$ are fast, slow and super-slow time scales. Then, the initial conditions are expressed as $\psi_1^x(0) = v_0/\omega$ and $\psi_1^y(0) = \psi_2^y(0) = 0$. In what follows, we omit the details of the CX-A analysis and provide a summary of the main results.

To this end, we transform Eq. (21), express the time derivatives in terms of the new time scales, and substitute the expansions (22). At the leading order, we obtain:

$$\psi_{10}^x = \varphi_{10}^x(\tau_1,\tau_2)\,e^{i\tau_0}, \qquad \psi_{10}^y = \varphi_{10}^y(\tau_1,\tau_2)\,e^{i\tau_0}, \qquad \psi_{20}^y = \varphi_{20}^y(\tau_1,\tau_2)\,e^{i\tau_0} \tag{23}$$

By imposing appropriate solvability conditions in the $O(\varepsilon)$ subproblem, we compute,

$$\begin{aligned}
\varphi_{10}^x(\tau_1,\tau_2) &= \mathrm{A}_1(\tau_2)\cos(\beta\tau_1) - i\mathrm{B}_1(\tau_2)\sin(\beta\tau_1)\\
\varphi_{10}^y(\tau_1,\tau_2) &= \mathrm{B}_1(\tau_2)\cos(\beta\tau_1) - i\mathrm{A}_1(\tau_2)\sin(\beta\tau_1)\\
\varphi_{20}^y &= \mathrm{B}_2(\tau_2)
\end{aligned} \tag{24}$$

with $\mathrm{A}_1(\tau_2)$, $\mathrm{B}_1(\tau_2)$ and $\mathrm{B}_2(\tau_2)$ being super-slowly varying complex amplitudes. Having eliminated its secular terms the resulting $O(\varepsilon)$ subproblem yields:

$$\psi_{11}^x = -\frac{\beta}{2}\overline{\varphi}_{10}^y(\tau_1,\tau_2)\,e^{-i\tau_0}, \quad \psi_{11}^y = -\frac{\beta}{2}\overline{\varphi}_{10}^x(\tau_1,\tau_2)\,e^{-i\tau_0}, \quad \psi_{21}^y = 0 \tag{25}$$

We then proceed to the $O\left(\varepsilon^2\right)$ subproblem to determine the super-slow amplitudes $\mathrm{A}_1(\tau_2)$, $\mathrm{B}_1(\tau_2)$ and $\mathrm{B}_2(\tau_2)$; this reads:

$$\begin{aligned}
&\frac{\partial\psi_{10}^x}{\partial\tau_2} + \frac{\partial\psi_{11}^x}{\partial\tau_1} + \frac{\partial\psi_{12}^x}{\partial\tau_0} - i\psi_{12}^x + \alpha\left[\frac{\left(\psi_{10}^x - \overline{\psi}_{10}^x\right)}{2i}\right]^3 = -i\beta\left(\psi_{11}^y - \overline{\psi}_{11}^y\right)\\
&\frac{\partial\psi_{10}^y}{\partial\tau_2} + \frac{\partial\psi_{11}^y}{\partial\tau_1} + \frac{\partial\psi_{12}^y}{\partial\tau_0} - i\psi_{12}^y + \alpha\left[\frac{\left(\psi_{10}^y - \overline{\psi}_{10}^y\right)}{2i} - \frac{\left(\psi_{20}^y - \overline{\psi}_{20}^y\right)}{2i}\right]^3 = -i\beta\left(\psi_{11}^x - \overline{\psi}_{11}^x\right)\\
&\frac{\partial\psi_{20}^y}{\partial\tau_2} + \frac{\partial\psi_{21}^y}{\partial\tau_1} + \frac{\partial\psi_{22}^y}{\partial\tau_0} - i\psi_{22}^y + \alpha\left[\frac{\left(\psi_{20}^y - \overline{\psi}_{20}^y\right)}{2i}\right]^3 + \alpha\left[\frac{\left(\psi_{20}^y - \overline{\psi}_{20}^y\right)}{2i} - \frac{\left(\psi_{10}^y - \overline{\psi}_{10}^y\right)}{2i}\right]^3 = 0
\end{aligned} \tag{26}$$

Substituting (23) and (25) into (26) and eliminating the resulting secular terms we obtain the *low-energy super-slow flow* governing $A_1(\tau_2)$, $B_1(\tau_2)$ and $B_2(\tau_2)$,

$$\begin{aligned}
\frac{dA_1(\tau_2)}{d\tau_2} &= \frac{\beta}{2\pi}\int_0^{\frac{2\pi}{\beta}} \left\{\left[-\frac{3i}{8}\alpha\left(-\left|\varphi_{10}^x\right|^2\varphi_{10}^x\right)-\frac{i\beta^2}{2}\varphi_{10}^x\right]\cos(\beta\tau_1)\right.\\
&\quad \left.+\, i\left[-\frac{3i}{8}\alpha\left(-\left|\delta_1^y\right|^2\delta_1^y\right)-\frac{i\beta^2}{2}\varphi_{10}^y\right]\sin(\beta\tau_1)\right\}d\tau_1\\
\frac{dB_1(\tau_2)}{d\tau_2} &= \frac{\beta}{2\pi}\int_0^{\frac{2\pi}{\beta}} \left\{\left[-\frac{3i}{8}\alpha\left(-\left|\delta_1^y\right|^2\delta_1^y\right)-\frac{i\beta^2}{2}\varphi_{10}^y\right]\cos(\beta\tau_1)\right.\\
&\quad \left.+\, i\left[-\frac{3i}{8}\alpha\left(-\left|\varphi_{10}^x\right|^2\varphi_{10}^x\right)-\frac{i\beta^2}{2}\varphi_{10}^x\right]\sin(\beta\tau_1)\right\}d\tau_1\\
\frac{dB_2(\tau_2)}{d\tau_2} &= \frac{\beta}{2\pi}\int_0^{\frac{2\pi}{\beta}} \left(-\frac{3i}{8}\alpha\right)\left(\left|\delta_1^y\right|^2\delta_1^y-\left|\varphi_{20}^y\right|^2\varphi_{20}^y\right)d\tau_1
\end{aligned} \tag{27}$$

where φ_{10}^x, φ_{10}^y and φ_{20}^y are expressed by (24), the initial conditions are $A_1(0+)=v_0/\omega$, $B_1(0)=B_2(0)=0$, and $\delta_1^y=\varphi_{10}^y-\varphi_{20}^y$. The right-hand-sides of (27) are averaged expressions with respect to the *slow time scale* τ_1, which in the method of multi-scales is treated as independent from the *super-slow time scale* τ_2. It can be shown that (27) admits the unique steady state solution $B_1(\tau_2)=B_2(\tau_2)=0$ and $A_1(\tau_2)\neq 0$ governed by:

$$\frac{dA_1(\tau_2)}{d\tau_2}=\frac{9i}{32}\alpha\left|A_1(\tau_2)\right|^2A_1(\tau_2)-\frac{i\beta^2}{2}A_1(\tau_2)\Rightarrow A_1(\tau_2)=\left|A_1(0)\right|e^{i\left(\frac{9\alpha}{32}\left|A_1(0)\right|^2-\frac{\beta^2}{2}\right)\tau_2} \tag{28}$$

From (28) note that $|A_1(\tau_2)|=|A_1(0)|$, which is a constant for $\tau_2\geq 0$. Combining the previous results, we express the slow modulations in the leading order approximations (23) as,

$$\begin{aligned}
\varphi_{10}^x(\tau_1,\tau_2) &= \left|A_1(0)\right|e^{i\omega_2\tau_2}\cos(\beta\tau_1)\\
\varphi_{10}^y(\tau_1,\tau_2) &= -i\left|A_1(0)\right|e^{i\omega_2\tau_2}\sin(\beta\tau_1)\\
\varphi_{20}^y &= 0
\end{aligned} \tag{29}$$

where $\omega_2=\frac{9\alpha}{32}|A_1(0)|^2-\frac{\beta^2}{2}$. Solution (29) yields a time-periodic or quasiperiodic response for the original ROM through (23). Hence, in the leading order approximation of the low energy Regime I the energy of oscillator A2 of the ROM is zero, and the energy is recursively exchanged between the two leading oscillators E1 and A1 in a nonlinear beat phenomenon. This corresponds to a localized oscillation in the two leading oscillators of the excited and absorbing lattices in the asymmetric network. As the intensity of the impulse increases though, a bifurcation occurs and the oscillator A2 starts gaining energy; in terms of the lattice model this signifies the process of breather initiation in the absorbing lattice and transition to Regime II.

To approximate this bifurcation analytically, we seek the condition for non-zero response of oscillator A2, i.e., $\psi_2^y\neq 0$. Given that $\psi_{20}^y=0$, we have that $\psi_2^y=\varepsilon\psi_{21}^y(\tau_0,\tau_1,\tau_2)+\varepsilon^2\psi_{22}^y(\tau_0,\tau_1,\tau_2)+\varepsilon^3\psi_{23}^y(\tau_0,\tau_1,\tau_2)+O\left(\varepsilon^4\right)$. Then, we derive,

$$\begin{aligned}
\psi_{21}^y &= \left[\frac{9\alpha}{32\beta}A_1(\tau_2)\left|A_1(\tau_2)\right|^2\cos(\beta\tau_1)-\right.\\
&\left.\frac{\alpha}{32\beta}A_1(\tau_2)\left|A_1(\tau_2)\right|^2\cos(3\beta\tau_1)+C(\tau_2)\right]e^{i\tau_0}
\end{aligned} \tag{30}$$

where the super-slowly varying term of integration, $C(\tau_2)$, is evaluated by eliminating secular terms from the $O\left(\varepsilon^3\right)$ subproblem governing the approximation $\psi_{23}^y(\tau_0,\tau_1,\tau_2)$:

$$\frac{\partial C(\tau_2)}{\partial\tau_2}=\frac{3}{16}\alpha i\left[-A_1^2(\tau_2)\overline{C}(\tau_2)+2\left|A_1(\tau_2)\right|^2C(\tau_2)\right] \tag{31}$$

Introducing the final transformation $C(\tau_2)=D(\tau_2)A_1(\tau_2)|A_1(\tau_2)|^2$ in (31) we derive,

$$\begin{aligned}
\frac{dRe(D)}{d\tau_2} &= -\frac{3}{32}\alpha\left|A_1(0+)\right|^2Im(D)-\frac{\beta^2}{2}Im(D)-\frac{3}{16}\alpha\left|A_1(0+)\right|^2Im(D)\\
\frac{dIm(D)}{d\tau_2} &= \frac{3}{32}\alpha\left|A_1(0+)\right|^2Re(D)+\frac{\beta^2}{2}Re(D)-\frac{3}{16}\alpha\left|A_1(0+)\right|^2Re(D)
\end{aligned} \tag{32}$$

where $|A_1(\tau_2)|=v_0/\omega$. From (32), and reverting back to physical (unscaled) initial velocity, the critical low-energy initial velocity is given by $(3\alpha/16)\left(\frac{v_{0,cr}^{LE}}{\omega}\right)^2=\varepsilon\beta^2$; for $v_0>v_{0,cr}^{LE}$ (32) becomes unstable and the response of oscillator A2 of the ROM grows, signifying the initiation of the breather in the asymmetric lattice network. For the previous system parameters this bifurcation is predicted at $v_{0,cr}^{LE}=0.0148$ m/s versus the numerical value of ~ 0.03 m/s (cf. Fig. 5). The discrepancy is due to the averaging operations in the CX-A analysis.

This completes the study of the low- and high-energy bifurcations that bound the LZT irreversible energy Regime II in Fig. 5. In the next section we show that irreversible energy transfer yields acoustic non-reciprocity in the asymmetric lattice network (3).

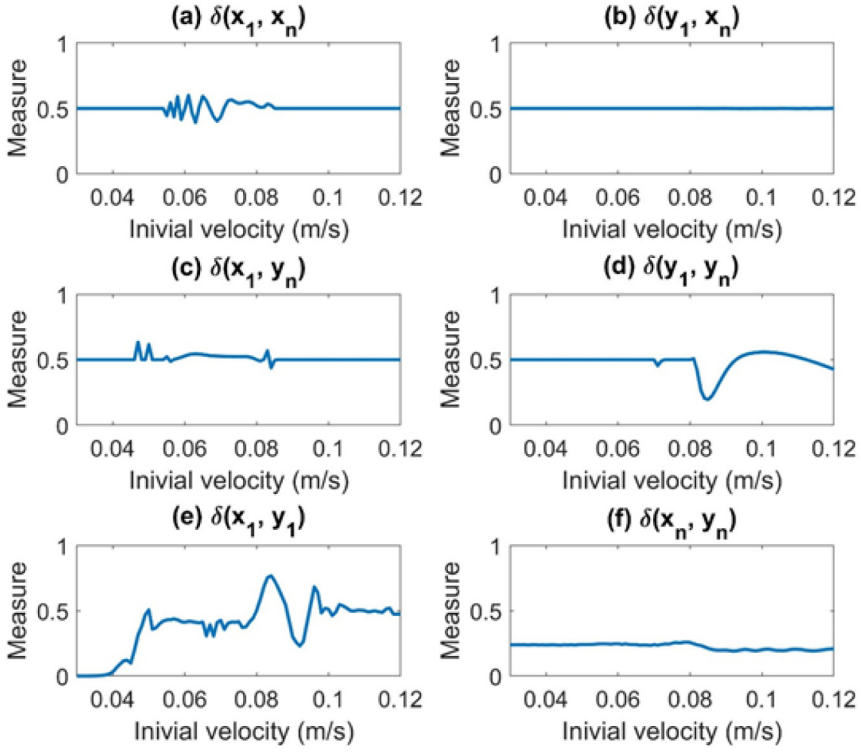

Fig. 11. Numerical non-reciprocity measures for the finite asymmetric lattice network as functions of the initial velocity v_0 (or equivalently, impulse intensity).

5. Acoustic non-reciprocity in the asymmetric lattice network

Reciprocity is a fundamental property in linear time-invariant (LTI) systems [21,22]. Breaking reciprocity involves time-variant system properties, external biases or nonlinearity [23]. However, as shown in [24] in addition to nonlinearity, asymmetry is also needed for Non-reciprocity. It is of interest to study the break of reciprocity in the asymmetric lattice network (2), so departing from the previous discussion we consider its *finite* version by assuming N oscillators in each lattice. Moreover, all boundaries of the finite network are traction-free.

We apply an impulse to each of the four free boundaries and study the resulting non-reciprocal dynamics by confining our attention exclusively to the reciprocity between any two boundary locations, say A and B. First we apply an impulse at A and measure the resulting response, $z_{AB}(t)$, at B; then we reverse the points of excitation and measurement, by applying the same impulse at B and measuring the response $z_{BA}(t)$ at A. If the nonlinear dynamics is reciprocal it should hold that $z_{AB}\,(t) = z_{BA}\,(t)\,, t \geq 0$. To quantify the non-reciprocity we propose a normalized measure similar in spirit of [24–26],

$$\delta\left[z_{AB}(t), z_{BA}(t)\right] = \frac{\int_0^T \left[z_{AB}\,(t) - z_{BA}(t)\right]^2 dt}{\int_0^T \left\{\left[z_{AB}\,(t) - z_{BA}(t)\right]^2 + \left[z_{AB}\,(t) + z_{BA}(t)\right]^2\right\} dt} \tag{33}$$

where T represents a sufficiently long time interval. Compared to previous works (33) has the advantage of not becoming singular when either z_{AB} or z_{BA} (but not both) approach small values (e.g., in cases of energy localization). In addition, δ satisfies $\delta\,(az_1, az_2) = \delta\,(z_1, z_2)$; it is positive definite $(\delta\,(z_1, z_2) \geq 0 \forall z_1, z_2 \neq 0)$; and obey the triangular inequality, $\delta\,(z_1, z_2) + \delta\,(z_2, z_3) \geq \delta\,(z_1, z_3)\,\forall z_1, z_2, z_3 \in R$. Therefore, $\delta\left[z_1(t), z_2(t)\right]$ represents a normalized measure of any two time series $z_1(t)$ and z_2(t), except when $z_1\,(t) = z_2(t) \equiv 0$. Moreover, $\delta \in [0, 1]$, with $\delta\,(z_1, z_2) = 0$ if and only if $z_1 \equiv z_2 \neq 0$, whereas $\delta\,(z_1, z_2) = 1$ iff $z_1 \equiv -z_2 \neq 0$. *Hence, the most non-reciprocal case is when* $z_{AB}\,(t) = -z_{BA}\,(t)\,, t \geq 0$.

We consider all six combinations of forcing-measurement locations for the finite asymmetric lattice network; e.g., one possible combination is to apply an impulse at the left boundary of the excited lattice, and measure the response at the right boundary the absorbing lattice, $y_N(t)$; then, to reverse the forcing-measurement locations and record the response at the left boundary of the excited lattice, $x_1(t)$. Then, the non-reciprocity measure $\delta\left[x_1(t), y_N(t)\right]$ is computed. In Fig. 11 we depict the six non-reciprocity measures as functions of the intensity of the applied impulse, where the time T is selected so that no reflections of the primary wave interfere with the computation. The system parameters of the asymmetric lattice network of Section 2 are used and $N = 20$ oscillators for each lattice are assumed.

Considering that the finite symmetric network is reciprocal, these results reveal the strong non-reciprocity caused by the local asymmetry due to spatial variation of the grounding stiffnesses of the exciting lattice. Hence, *the combination of strong nonlinearity and local asymmetry yields global non-reciprocity in the network with spatial variation*. The only case of reciprocal behavior is for $\delta\left[x_1(t), y_1(t)\right]$ when $v_0 < 0.04$ m/s, since this corresponds to the localized solution in Regime I. In all other cases the dynamics is non-reciprocal with stronger non-reciprocity achieved for $\delta\left[x_1(t), y_1(t)\right]$ in Regimes II, III, and IV, i.e., at the locations closest to the spatial variation of the stiffnesses, and weaker in $\delta\left[x_N(t), y_N(t)\right]$, i.e., at the locations farthest from the spatial variation of the stiffnesses. These results

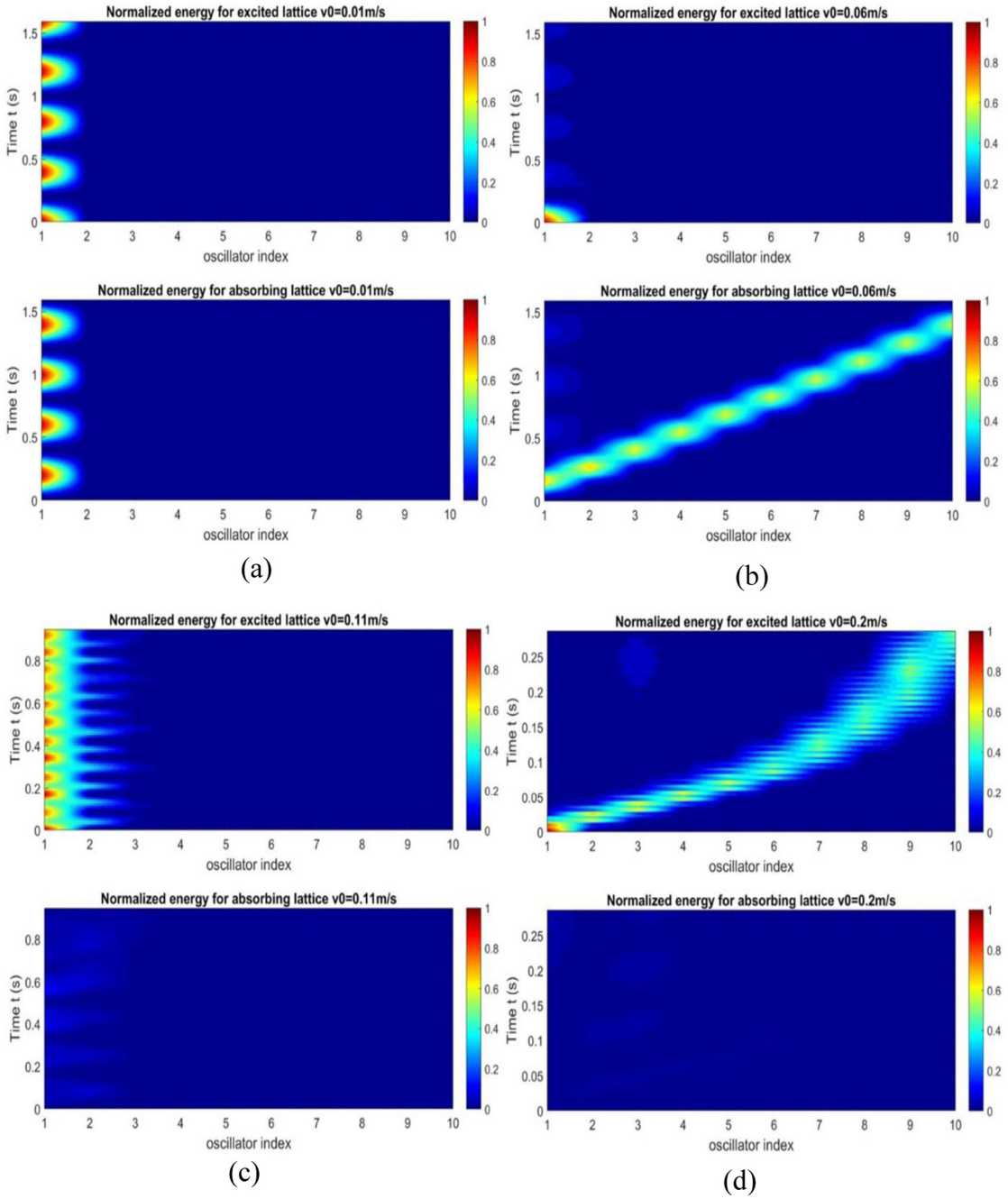

Fig. A.1. Spatio-temporal evolutions of the normalized energies of the two lattices of the asymmetric network revealing the strong dependence of the nonlinear acoustics on energy: (a) $v_0 = 0.01$ m/s (Region I), (b) $v_0 = 0.06$ m/s (Region II), (c) $v_0 = 0.11$ m/s (Region III) and (d) $v_0 = 0.20$ m/s (Region IV).

agree with prior works on nonlinear, asymmetric lattices, e.g., [26]. Finally, the most common non-reciprocity measure is equal to 0.5, indicating that the two corresponding responses are "orthogonal". That is, in the regime of irreversible energy transfer, if we apply the impulse at location A, we measure the non-zero response $z_{AB}(t)$ at location B. Alternatively, if we apply the same impulse at location B, and the response at location A is $z_{BA}(t) = 0$, then the non-reciprocity measure is equal to 0.5 since the zero response is "orthogonal" to any non-zero response.

6. Concluding remarks

We studied passive irreversible energy transfer (redirection) and localization in a weakly coupled network of nonlinear lattices with a local spatial asymmetry. In the absence of asymmetry energy is exchanged recurrently between the lattices of the network through propagating breathers. A *local* asymmetry induces *global* effects in the acoustics of this network, i.e., irreversible energy transfer. A reduced-order analysis proves that this is caused by the spatial macroscopic analogue of the Landau–Zener tunneling (LZT) temporal quantum effect. The asymptotic energy distribution between the two lattices of the network is predicted analytically and agrees well

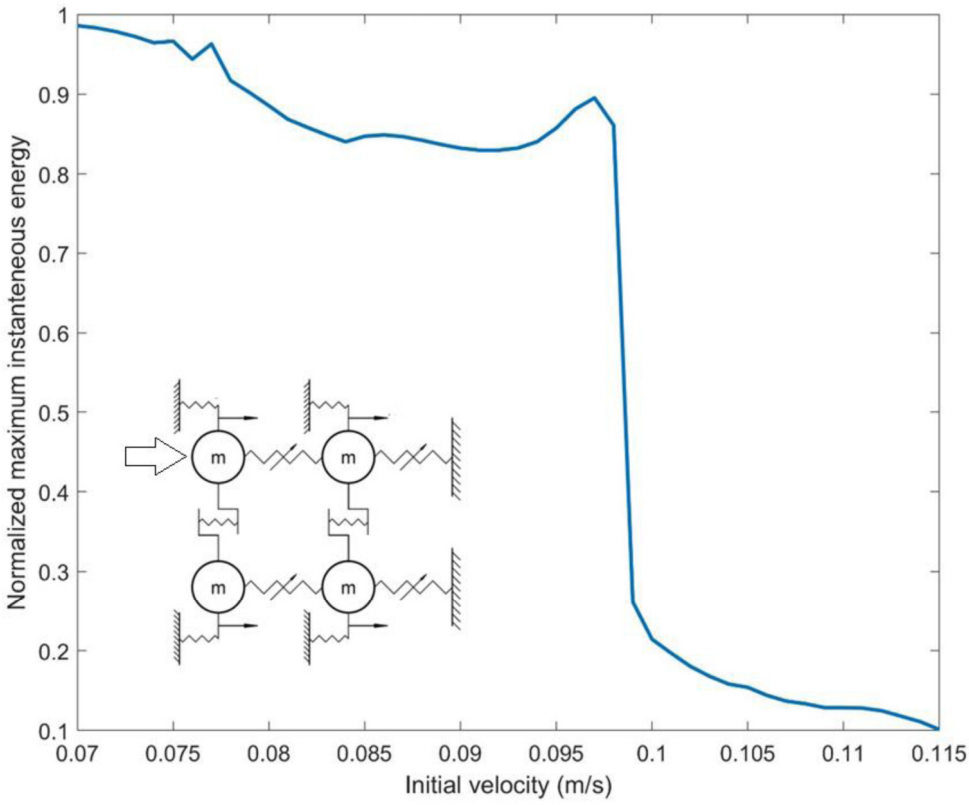

Fig. B.1. Normalized maximum instantaneous energy in the two absorbing oscillators of the four-DOF ROM as function of the initial velocity v_0 (intensity of the impulse).

with the numerical results. In addition, the critical role of the intensity of the applied impulse (energy) is clarified by constructing and analyzing appropriate reduced-order models (ROMs), valid either in the low- or the high-energy regimes. The asymptotic analysis of these ROMs proves that the LZT effect only occurs within a critical finite energy band, and outside it energy localization takes place. Physical insight is provided on the nonlinear mechanisms governing the transition from localization to irreversible energy transfer as energy varies, as well as, on the bifurcations that bound the critical energy band of the LZT effect. Finally, the repercussions in terms of non-reciprocity in the nonlinear dynamics of the finite lattice network are discussed, by numerically showing that the local spatial asymmetry yields strong break of reciprocity in the global dynamics.

The potential applications of LZT-based passive energy redirection in structural networks are diverse. These include, nonlinear acoustic metamaterials with the capacity of inherent energy redirection to preferential, *a priori* designated paths, yielding improved passive mitigation against shocks or blasts; nonlinear structural networks that are self-adaptive to energy, and thus capable of changing their responses depending on the intensity or type of the applied broadband excitations; and non-reciprocal passive arrays of oscillators enabling uni-directional sound transmission, and capacity for enhanced acoustic isolation.

Acknowledgments

This work was supported in part by the National Science Foundation, United States of America under NSF EFRI Grant No. 1741565. The authors acknowledge insightful discussions with Jonathan Bunyan and Alireza Mojahed.

Appendix A. Spatio-temporal plots in different regimes

Here we include the spatio-temporal energy distributions in each of the four robust Regions depicted in Fig. 5 for initial velocities $v_0 = 0.01, 0.06, 0.11$ and 0.20 m/s, highlighting the strong dependence of the nonlinear acoustics on energy.

It is clearly shown from Fig. A.1 that the Region II (Subfigure b) corresponds to the LZT in space (passive energy redirection), whereas the energy is localized in the leading oscillators in both Region I and III. For Region IV, the energy propagates along the excited lattice with few energy transferred from the excited lattice to the absorbing lattice.

Appendix B. Numerical results for the 4-DOF ROM

In order to improve our results of the high-energy, we consider a 4-DOF ROM composed of the two leading oscillators of the excited and absorbing lattices of the asymmetric network of Fig. 3– that is, there are two excited and two absorbing oscillators. An interesting added feature of this ROM compared to the simplified two-DOF ROM of Fig. 8, is that it now incorporates the stiffness reduction rate γ in the grounding stiffness of the second oscillator of the excited lattice. In this case, we perform a numerical study instead of analytical work to determine the critical initial velocity corresponding to the aforementioned bifurcation.

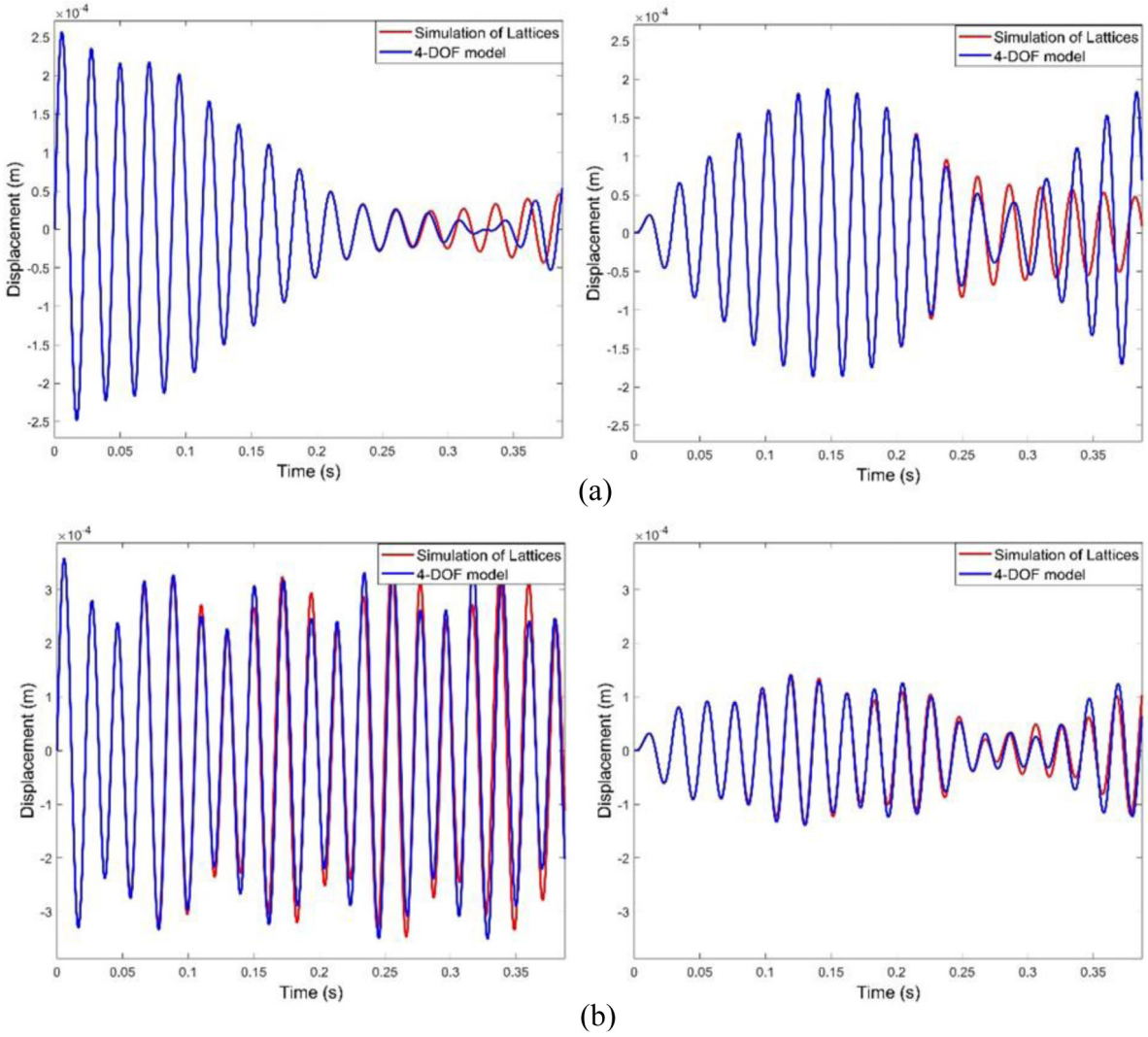

Fig. B.2. Comparison of the exact responses derived by the full model (3) (red lines) to the responses predicted by the four-DOF ROM (blue lines) for: (a) $v_0 = 0.07$ m/s $< v_{0,cr}^{HE}$, and (b) $v_0 = 0.1$ m/s $> v_{0,cr}^{HE}$; in each case the left (right) plot depicts the response of the leading excited (absorbing) oscillator. (For interpretation of the references to color in this figure legend, the reader is referred to the web version of this article.)

In particular, for fixed initial velocity v_0 we compute the maximum instantaneous energy attained by the two absorbing oscillators and normalized with respect to the initial energy provided by the impulse. Moreover, all system parameters are identical to the ones of the asymmetric lattice network corresponding to the plots of Fig. 5. In Fig. B.1 this energy measure is plotted as function of v_0, from which the critical initial velocity in the high-energy regime is estimated as $v_{0,cr}^{HE} \approx 0.098$ m/s which is an improvement compared to the previous two-DOF ROM. The validity of the four-DOF ROM is confirmed by the plots of Fig. B.2 where the predicted responses of the leading excited and absorbing oscillators are compared to the exact numerical responses of the full asymmetric network model (3) for initial velocities below and above the predicted bifurcation value. Good agreement is noted, especially at earlier times, which indicates that the considered ROM is capably of capturing the bifurcation between irreversible energy transfer and localization in the acoustics of the asymmetric lattice network. This concludes the discussion of the high-energy bifurcation between Regimes II and III in Fig. 5.

References

[1] R.K. Dodd, H.C. Morris, J. Eilbeck, J. Gibbon, Solitons and Nonlinear Wave Equations, Academic Press, London and New York, 1982.
[2] S. Flach, K. Kladko, Moving discrete breathers? Physica D 127 (1999) 61–72.
[3] G. James, Nonlinear waves in Newton's Cradle and the discrete P-Schrödinger equation, Math. Models Methods Appl. Sci. 21 (2011) 2335–2377.
[4] G. James, Y. Sire, Travelling breathers with exponentially small tails in a chain of nonlinear oscillators, Comm. Math. Phys. 257 (2005) 51–85.
[5] Y. Sire, G. James, Travelling breathers in Klein–Gordon chains, C. R. Math. 338 (2004) 661–666.
[6] M.A. Hasan, S. Cho, K. Remick, A.F. Vakakis, D.M. McFarl, W.M. Kriven, Experimental study of nonlinear acoustic bands and propagating breathers in ordered granular media embedded in matrix, Granul. Matt. 17 (2015) 49–72.
[7] Y. Zhang, D.M. McFarland, A.F. Vakakis, Propagating discrete breathers in forced one-dimensional granular networks: Theory and experiment, Granul. Matt. 19 (2017) 59.
[8] Y. Zhang, K.J. Moore, D.M. McFarland, A.F. Vakakis, Targeted energy transfers and passive acoustic wave redirection in a two-dimensional granular network under periodic excitation, J. Appl. Phys. 118 (2015) 234901.

[9] Y. Starosvetsky, M.A. Hasan, A.F. Vakakis, L.I. Manevitch, Strongly nonlinear beat phenomena and energy exchanges in weakly coupled granular chains on elastic foundations, SIAM J. Appl. Math. 72 (2012) 337–361.
[10] L.I. Manevitch, New approach to beating phenomenon in coupled nonlinear oscillatory chains, Arch. Appl. Mech. 77 (2007) 301–312.
[11] K.R. Khusnutdinova, D.E. Pelinovsky, On the exchange of energy in coupled Klein–Gordon equations, Wave Motion 38 (2003) 1–10.
[12] M.A. Hasan, Y. Starosvetsky, A.F. Vakakis, L.I. Manevitch, Nonlinear targeted energy transfer and macroscopic analog of the quantum Landau–Zener effect in coupled granular chains, Physica D 252 (2013) 46–58.
[13] C. Zener, Non-adiabatic crossing of energy levels, Proc. R. Soc. Lond. Ser. A 137 (1932) 696–702.
[14] M. Razavy, Quantum Theory of Tunneling, World Scientific Press, Singapore, 2003.
[15] L.I. Manevitch, Y.A. Kosevich, M. Mane, G. Sigalov, L.A. Bergman, A.F. Vakakis, Towards a new type of energy trap: Classical analog of quantum Landau–Zener tunneling, Int. J. Non-Linear Mech. 46 (2013) 247–252.
[16] A. Mojahed, A.F. Vakakis, Certain aspects of the acoustics of a strongly nonlinear discrete lattice, Nonlinear Dyn. (2019) 1–17.
[17] A. Mojahed, J. Bunyan, S. Tawfick, A.F. Vakakis, Tunable acoustic non-reciprocity in nonlinear asymmetric waveguides, Phys. Rev. Appl. 12 (3) (2019) 034033.
[18] L.I. Manevitch, Complex Representation of Dynamics of Coupled Nonlinear Oscillators, in Mathematical Models of Non-Linear Excitations: Transfer, Dynamics, and Control in Condensed Systems and Other Media, Kluwer Academic, Plenum Publishers, New York, 1999.
[19] A.H. Nayfeh, D. Mook, Nonlinear Oscillations, Wiley Interscience, NY, 1985.
[20] M. Abramowitz, L.A. Stegun, Handbook of Mathematical Functions, Dover, New York, 1974.
[21] H.V. Helmholtz, Theorie der Luftschwingungen inRöhren mit offenen Enden, J. für die Reine Ang. Math. 57 (1860) 1.
[22] J.W. Strutt, Some general theorems relating to vibrations, Proc. Lond. Math. Soc. 1 (1) (1871) 357–368.
[23] R. Fleury, D. Sounas, M.R. Haberman, A. Alu, Nonreciprocal acoustics, Acoust. Today 11 (3) (2015) 14–21.
[24] A. Blanchard, T.P. Sapsis, A.F. Vakakis, Non-reciprocity in nonlinear elastodynamics, J. Sound Vib. 412 (2018) 326–335.
[25] C.A. Herrera, D.M. McFarland, L.A. Bergman, A.F. Vakakis, Methodology for nonlinear quantification of a flexible beam with a local, strong nonlinearity, J. Sound Vib. 388 (2017) 298–314.
[26] J. Bunyan, K.J. Moore, A. Mojahed, M.D. Fronk, S. Tawfick, M.J. Leamy, A.F. Vakakis, Acoustic non-reciprocity in a lattice incorporating nonlinearity, asymmetry and internal scale hierarchy: Experimental study, Phys. Rev. E 97 (2018) 052211.